Subsidence analysis, maturity modelling and hydrocarbon generation of the Alpine sedimentary sequence in the NW of the Iberian Ranges (Central Spain)

A.RAMOS*, A. SOPEÑA*, Y. SÁNCHEZ-MOYA*, and A. MUÑOZ**

* Instituto de Geologia Economica-Departamento de Estratigrafia, *Universidad Complutense, 28040 Madrid Spain*
** Instituto Español de Oceanografia, Corazon de Maria 8, 28002 Madrid Spain

RESUMEN

A partir de los datos geológicos disponibles, se ha realizado la modelización computerizada de la evolución térmica y de la generación de hidrocarburos de la sucesión sedimentaria pérmico-terciaria en el NW de la Cordillera Ibérica. El análisis de la subsidencia indica que existen cuatro estadios diferenciados en la evolución Mesozoica de este área durante el ciclo de sedimentación Alpino. Estas cuatro etapas corresponden al Pérmico superior, Triásico, Jurásico inferior y medio, y Jurásico superior-Cretácico medio. Las diferencias observadas en las curvas de subsidencia tectónica obtenidas, permiten diferenciar cuatro dominios de extensión/elevación. Estos dominios de extensión/elevación se definen como bloques limitados por fallas donde se han registrado similares procesos extensionales y/o de elevación en un mismo estadio tectónico. Los dominios de extensión/elevación muestran la propagación areal de los procesos tectónicos a través del tiempo. Durante los tres primeros estadios evolutivos, se produce una extensión gradual a partir de un dominio central hacia el noreste y posteriormente hacia en suroeste. En el estadio Cretácico la tendencia de propagación se invierte. El flujo de calor en la base de la sucesión y la historia térmica del área, han sido reconstruidos empleando diferentes modelos de distribución del flujo de calor. La maduración térmica de la materia orgánica ha sido evaluada tentativamente, adoptando diferentes flujos de calor. Los resultados obtenidos se corresponden con los datos hasta ahora conocidos del área.

Palabras clave: Cordillera Ibérica, simulación numérica, subsidencia tectónica, flujo de calor, generación de hidrocarburos

Cuadernos de Geología Ibérica, núm. 21, pp. 23-53.
Servicio de Publicaciones. Universidad Complutense, Madrid, 1996.

ABSTRACT

The burial, thermal and hydrocarbon histories of late Permian-Tertiary sedimentary succession in the NW of the Iberian Ranges were investigated using a single-well model. The reconstructed geohistories indicate four stages of evolution during early Alpine to late Alpine infill in the studied area: late Permian, Triassic, early and middle Jurassic, and latest Jurassic-middle Cretaceous. The differences between interpreted basement behaviour interpreted from tectonic subsidence curves differentiates four major «rift-uplift realms». The «rift/uplift» realm is defined either as an individual fault-bounded structural domain of the continental phase of the rift system or as an uplift that displays similar extensional/uplift processes. These «rift/uplift realms» show a propagation of rifting/uplift stages through time. The initial Permian, Triassic and Jurassic episodes show a north-eastern propagation followed by a south-western propagation from the Central realm. Each of these realms shows also a gradual north-eastern progress of the extension strain. The Cretaceous rift/uplift stage seems to behave in the opposite direction. Present day bottom heat flow and thermal history were modelled, using both a steady state thermal and a paleothermal heat flow-invariant model. The present average bottom heat flow obtained falls within the range of values reported in the literature from similar tectonic contexts. Different heat flow values were tentatively adopted to determine maturation. All the quantitative estimations of generated hydrocarbons indicate that insignificant volumes of hydrocarbons were generated by source rocks considered in this study.

Key Words: Iberian Ranges, numerical simulation, subsidence, rift/ uplift realm, heat flow, hydrocarbon generation.

INTRODUCTION

The occurrence of oil and gas in sedimentary basins results from the complex dynamic interaction of several processes. During the last few years maturity models have become a standard tool to evaluate the timing and amount of hydrocarbon occurrence in a basin (Ungerer *et al.*, 1990; Waples, Suizu & Kamata, 1992 a & b; Williamson, 1992). These numerical simulation models seek to evaluate basin subsidence, thermal evolution and conversion of these into organic maturation and generation histories. The accuracy and predictive ability of these models depend largely on the quantity and quality of the data available and the validity of assumptions made during the model construction (Waples *et al.*, 1992b).

Basin modelling addresses a variety of physical and chemical phenome-

na: 1) Backstripping permits evaluation of the basin structural origin through the characterisation of subsidence rate. 2) Emulated present day heat flow and ancient geothermal gradients, from imposed heat flow or geothermal gradient at the base of the sedimentary column, provide a better understanding of the structural models of the basin development. 3) The time-temperature histories and Arrhenius law permit modelling the first order kerogen breakdown to evaluate organic maturity and estimate hydrocarbon generation.

The model described in this paper requires the input of some geological parameters that are imperfectly known. There are some large uncertainties in the geological and geochemical data used when calibrating the model. Uncertainties affect also the paleo-reconstruction of the heat flow, the timing of uplift, and the amount of sediment removed by erosion. Specific details can be controversial but do not obscure the main purpose of this paper: to establish a model of the process of hydrocarbon generation.

REGIONAL GEOLOGICAL FRAMEWORK

The model has been applied to a broad area from Central Spain (fig. 1a) that comprises several structural elements that together reflect a long and complex tectonic history.

During the late Variscan-late orogenic extensional stage (middle Carboniferous-early Permian) Central Iberia collapsed gravitationally. An important NW-SE fault system developed in the interior of the Iberian Plate and associated volcanic rocks were accumulated. Tectonic activity decreased during the Permian with the deposition of Saxonian facies. The early Alpine configuration of the Iberian Peninsula resulted into two contrasted realms: a Western Variscan block, and an Eastern Alpine block subject to post-orogenic extension (Doblas *et al.*, 1994a). During the early Alpine stage (fig. 1b) (Permian to Triassic) the Eastern Alpine realm might have developed a system of half-grabens involving listric/low angle detachments (Sanchez-Moya *et al.*, 1992). They were filled by hundreds of meters of red beds (Sopeña *et al.*, 1988). During the late Variscan to early Alpine stage (fig. 1b) the Iberian Peninsula can be related to an intracontinental dextral transcurrent shear zone (Arthaud & Matte, 1977) that probably represents the initial break up of the central part of Pangea (Doblas *et al.*, 1994b). The Iberian microplate lay between the African and American-European plates. With the onset of the Alpine cycle, the Iberian Plate underwent extension because of its location between two broad rifts and /or wrench areas, the Tethys and the Central Atlantic-Caribbean (Ziegler, 1990). During late Triassic and early Jurassic times, the subsidence was locally accompanied by volcanism (Sopeña *et al.*, 1988).

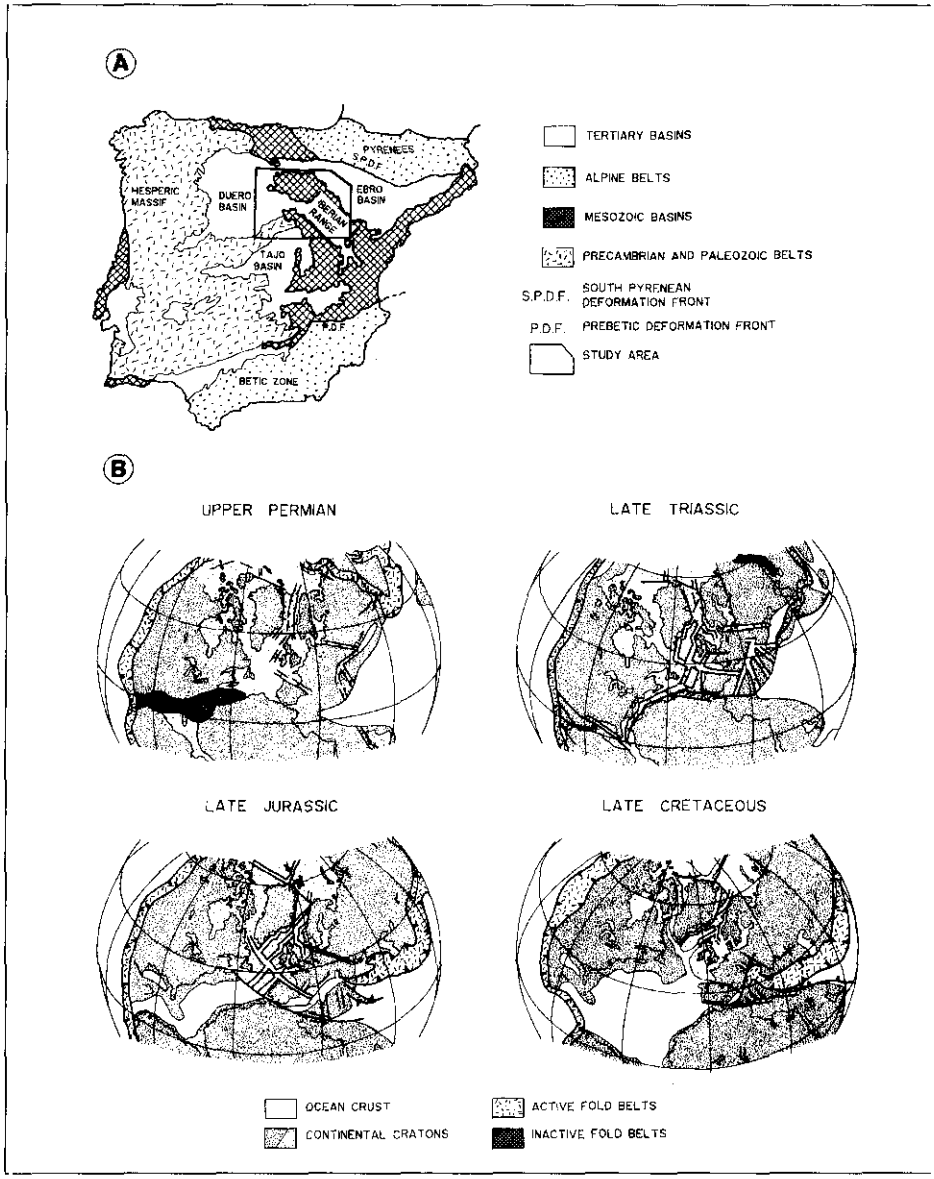

Figure 1a.—Simplified structural map of Iberia.
Figura 1a.—Mapa estructural de la Península Ibérica.
Figure 1b.—Tentative reconstruction of continent in Western hemisphere during Middle Permian to Late Cretaceous (after Ziegler, 1990).
Figura 1b.—Reconstrucción paleogeográfica del Hemisferio Occidental durante el Pérmico medio-Cretácico superior (Modificado de Ziegler, 1990)

Because of its location, the evolution of the Iberian plate, during late Jurassic-early Cretaceous (fig. 1b) was affected by the orthogonal opening of the Central Atlantic and the continuous floor spreading of the Bay of Biscay paralleled by a commensurate sinistral translation between Africa and Europe. This was coupled with late Jurassic sea floor spread in the West Tethys basins.

During the early Cretaceous, the North Atlantic area was probably affected by progressive lithospheric thinning in response to its mechanical stretching and thermal attenuation. The related thermal doming effect is particularly evident in Central Iberia. Neocomian to early Aptian crustal stretching between Newfoundland and Iberia limited sea-floor spreading between the Grand Banks and Portugal causing commensurate sinister translation into the Bay of Biscay. Contemporaneous wrench deformation is evident in the Iberian Ranges. During the late Aptian and Albian, Iberia began to rotate in a sinistral counter-clockwise away from the Armorican Margin (Ziegler, 1990).

During the Alpine cycle, after the extensional episode, a compressional stage developed. Late Paleocene compressional deformation is also evident in Iberia. Both are the expression of the collision of Iberia with the European Craton. It is likely that the build up of intra-plate compressional stress related to early Pyrenean collision resulted in large scale lithospheric deflection that disrupted the latest Cretaceous carbonate platforms that had occupied most of Iberia.

Dextral translation between Eurasia and Africa gained importance during late Alpine orogenic phases. The time span 50 My to 15 My corresponds to the collisional phase during which extra Iberia units collided with the southern Iberia margin (Betic front). During the late Eocene and Oligocene the Valencia rift system came into evidence. During the Miocene, crustal shortening persisting in the Betic Cordillera and the Maghrebian fold belt, was accompanied by the accentuation of the Gibraltar orocline.

The effects of compression can be observed in the study area. The intraplate deformation in Iberia resulted into two broad realms: The Iberian Range and the Hesperic Massif (fig. 1a). The Iberian Range corresponds to the deformation of the aulacogenic realm that deformed the thinned crustal area (Alvaro, Capote & Vegas, 1979). The more rigid areas in the interior of Iberia were deformed in great arches, that form the major physiographic features, bounded by reverse faults. Two large intraplate basins, the Tajo and Duero Basins, were formed in close connection with theses arches, and subsequently filled up by continental sediments.

Overall, the Neogene and Quaternary evolution of Iberia corresponds to a Post-Alpine extensional stage. This applies to both the Western Mediterranean and the intramontane basin. However the Valencia Trough and the Alboran Basin are two main prominent tensional structures that characterise the evolution of the Eastern and Southern margin of Iberia.

METHODS

A numerical simulation program, MATOIL, developed on VAX systems by the «Institute Francais du Petrole» (IFP), and adapted to the personal computer by BEICIP-FRANLAB, has been applied in this study to a broad area in Central Iberia (fig. 1a). The main data and assumptions are summarised in table I.

Subsidence analysis, thermal data, temperature parameters and thermal history have been carried out in this study, to evaluate the maturation of organic matter.

Subsidence analysis and compaction history

The local isostatic backstripping method (Steckler & Watts, 1978) for burial reconstruction and basin subsidence has been used. The thickness reconstruction is done using the Perrier and Quiblier (1974) method, which assumes that the amount of solid matrix remains constant. In the approach used here, the thickness of a formation is reduced according to its porosity-depth curve. Paleowater depths and eustatic sea-level corrections have not been necessary as sediments were deposited either in a shallow marine or in a continental environment.

In the interpretation of subsidence curves, Airy isostasy was assumed, thus ignoring the effect of a lithosphere finite strength on its response to sediment loading.

Analysis of thermal data and temperature parameters

The main conceptual assumptions to model past geothermal regimes and reconstruction of thermal history are based in the following ideas. 1) Temperature evolution in sediments depends on the input into the basin (basal heat flow), the heat transfer, and the redistribution through the sediments. 2) The temperature distribution within a sedimentary basin is the result of heat transfer from the mantle towards the Earth surface. 3) The study assumes that the total heat transfer can be expressed as follows: Total heat transfer = Heat flow + Heat source or storage. Where Heat flow = Geothermal Gradient x Conductivity + Heat carried by moving fluids. 4) The thermal conductivities and heat source or storage (radiogenic heat production and heat capacity) were automatically assigned by the computer program to each rock unit from its lithology, porosity and temperature. 5) The critical parameter for temperature in basin analysis is the basal heat flow. Basal heat flow has two components; radiogenic contribution of the crust and subcrustal heat flow that are not differentiated by the program. 6) Paleotemperatures are

Observational Data	Source	Utility
Age/depth-biostratigraphy lithology	Adell *et al.*, 1981a & b, 1982 Alonso *et al.*, 1982 Alonso Gavilán *et al.*, 87 Alonso, 1981 Ancochea *et al.*,1994 Arribas, 1984 Aurell, 1990 Barron & Goy, 1994 Caballero *et al.*, 1994 Capote *et al.*, 1982 Clemente & Alonso, 1990 Floquet, *et al.*, 1982	*Geometry of the sedimentary colum along basin history *Burial history compactation corrections *Burial history for each source rock
(PC, Personal Communication)	García Quintana, PC Gómez Fernández, J. C., 1992 & PC Gómez Fernández, J. J., PC Goy & Márquez-Aliaga, 1994 Goy & Martínez, 1994 Goy & Yebenes, 1977 Guiraud & Seguret, 1985 Hernando, 1977 Hernando & Rincón, 1987 Lagó *et al.*, 1994 Mas, PC Muñoz, 1993 Pérez-Mazario, 1990 Pocovi *et al.*, 1988 Quintero *et al.*, 1981 Ramos, 1979 Ramos *et al.*, 1986 Salvany, 1990 Segura & Wiedmann, 1982 Sopeña, 1973 Sopeña *et al.*, 1977 Vázquez, 1981 Wilde, 1990	*Density, Matrix conductivity, Matrix heat capacity *Thermal history
Botton hole temperatures	Well History reports Log Header information	Calibration against present day thermal data
Vitrine reflectance	Shell internal reports	Used only to compare to model predictions

Model Assumptions	Results
Local isostatis compensation (Airy Model) Initial porosities Decompaction factors	Compute porosity reduction and decompaction Subsidence curves
Thermal conductivity Thermal history —Constant heat flow —Variable heat flow —Rifting heat flow —Geothermal gradient Thermal properties of lithologies	Computation of thermal histories
Kinetic model	Maturity profiles (Transformation ratio, HI, Vitrinite reflectance, Tmax, SI, Prod. Index...) Amounts of generated oil and gas from each source rock vs geologic time

Table I.—NW Iberian Ranges maturity models: data and assumptions.
Tabla I.—Síntesis de los datos y parámetros empleados en la cuantificación numérica de la generación de hidrocarburos en el área NW de la Cordillera Ibérica.

controlled by the basal heat flow history of the basin, which reflects the lithosphere mechanics, but also by variations in thermal conductivities, heat capacity, heat generation from radioactive source within the sediments and regional water flow through aquifer.

Analysis of thermal history

In this study, the reconstruction of the temperature history of the sediments has required two steps.

1) Thermal histories of the heat flow have to define. Values of heat flow depend on the geodynamic setting of the basin. They can be either constant (when heat flow has not changed through time), variable (when tectonic setting has varied through time) or rifting heat flow (when heat flow is multiplied by extension rate).

2) To fit present day thermal state from available data.

Petroleum generation kinetic model

Conversion of the time and temperature histories into estimates of organic maturity was made through multiple parallel reactions governed by the first-order kinetics and the Arrhenius law. The mechanics of this approach are

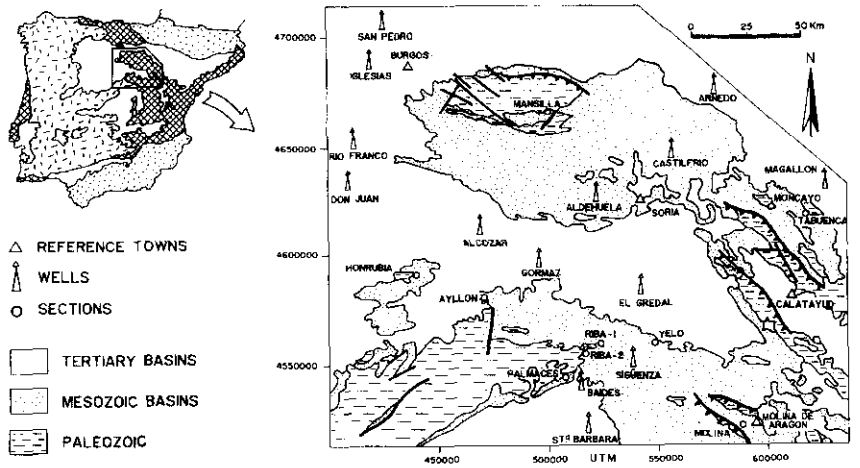

Figure 2.—Simplified geological map of the study area, showing the locations of wells and dummy wells (field sections) used in this study.

Figura 2.—Mapa geológico simplificado del área estudiada, mostrando la situación de los sondeos y columnas de campo analizados.

broad described in Tissot, Pelet & Ungerer, (1987) and Ungerer *et al.*, (1990). In this study primary cracking is considered with several parallel independent reactions. The rate of petroleum generation by each reaction is proportional to a constant rate which increases with temperature according to the Arrhenius law. Every primary reaction has its own activation energy and pre-exponential factor. The kinetic parameters used to model are derived from specific pyrolysis experiments (Ungerer & Pelet, 1987; Espitalié *et al.*, 1988; Evans & Felbeck, 1983; Castelli *et al.*, 1990) to account for the main organic types or subtypes. These kinetic parameters characterise the mode of primary cracking together with the initial potential of each reaction.

Three fractions are considered: C6+ (oil) unstable; C1-C5 (gas) stable; coke (solid carbon residue) stable. The total amount of petroleum that can be generated in a complete evolution depends on the initial amount of kerogen in the source rock, quantified by the TOC (Total Organic Carbon), and the petroleum potential of the kerogen.

Finally modelling maturity indicators are essential as they allow some quantitative controls of the model results by mean of geochemical data and must be compared with objective data available. The model computes the expected Hydrogen Index (HI), the Transformations Ratio (TR), the Vitrinite Reflectance (Ro) and the Temperature of Peak Petroleum Generation (Tmax).

SUBSIDENCE ANALYSIS

Fourteen wells and ten pseudo wells constructed from outcrop sections were used to quantify the compaction, subsidence, thermal history and maturity computations (fig. 2). The stratigraphy and age of each formation are given in fig. 3. The ages are not tightly constrained and the «2 My error» has been assumed. The most representative water balanced tectonic subsidence curves determined from all the wells and sections of the basin without sea level and/or paleobathymetry corrections are shown in fig. 4.

When observing figure 4, the essential characteristics of the subsidence history have been clearly recorded in all diagrams. However, not all the events can be recognised throughout the basin. The differences between the tectonic subsidence curves performed have permitted separation into different realms by each rifting and /or uplift stage. Based on the rift segment idea of Nelson, Patton & Morley (1992), we propose the term of «rift/uplift realm.» This rift/uplift realm is defined as an individual fault-bounded structural domain of the continental phase of the rift system or uplift that displays similar extensional/uplift processes.

A first episode of rifting/uplift occurred during Permian (285 to 250 My). The tectonic subsidence curves (figs. 4 a, b, c) determine a Central Realm

(C.R. in fig. 5a). This realm is characterised by a steep initial downward-trending segment (285 to 270 My) interpreted like a crustal thinning and normal faulting. The Central Realm shows the maximum Permian thickness. This episode resulted in the formation of a complex system of small and isolated NW-SE trending half grabens filled by hundreds of meters of red beds during late Permian. This period of subsidence was followed by a period of uplift and erosion resulting in a disconformity between Saxonian facies and late Permian-early Triassic Buntsandstein facies (270 to 250 My).

A second stage of rifting/uplift took place roughly during Triassic (fig. 4). The base of late Permian and/ or early Triąssic sedimentary strata (Buntsandstein facies base) subsided at a relative high rate through the deposition of Buntsandstein and Muschelkalk facies (≃ 250 to ≃ 230 My), followed by a pseudo-exponential or linear form of the late Triassic-early Jurassic subsidence (Keuper facies and base of the *Carniolas de Cortes de Tajuña* Formation, ≃ 230 to ≃ 210 My). The rapid initial subsidence phase is associated to rifting of the crust and thinning of the sub-crustal lithosphere. This phase is followed by a thermal subsidence phase (pseudo-exponential shape) associated to the thermal contraction and cooling of the lithosphere. This rifting period can be related to the late Variscan to early Alpine stage on the Iberian Peninsula that might represent the initial break up of the central part of Pangea.

Figure 3.—Composite lithostratigraphic framework of NW Iberian Ranges study area. Locations given in figure 2. Source data summarised in table I. EB: Ermita Beds. MB: Montesoro Beds. B: Buntsandstein facies. M: Muschelkalk facies. K: Keuper facies. RG: Renales Group comprising from bottom to top; Dolomías tableadas de Imón, Carniolas de Cortes de Tajuña and Calizas y dolomías tableadas de Cuevas Labradas formations. AG: Ablanquejo Group comprising from bottom to top; Margas grises del Cerro del Pez, Calizas bioclásticas de Barahona and Alternancia de Margas y calizas de Turmiel. CH: Carbonatos de Chelva and Margas de Sot de Chera formations. HV: Huerteles and Valdeprado formations. T: Aldealpozo and Torrecilla formations. SM: Sierra Matute formation. OG: Oncala Group, comprising from bottom to top; Sierra Matute, Huerteles and Valdeprado formations. ML: Malacara formation. A: Abejar formation. U: «Utrillas» facies. P: Stª María de las Hoyas, Picofrentes and Muñecas formations. DS: Hortezuelas, Hontoria del Pinar, Burgo de Osma, Santo Domingo de Silos and Santibáñez del Val formations. PG: Paleogene. N: Neogene.

Figura 3.—Esquema litoestratigráfico del NW de la Cordillera Ibérica. La localización y la fuente de los datos empleados vienen dados en la figura 2 y tabla I respectivamente. EB: Capas de la Ermita. MB: Capas de Montesoro . B: Facies Buntsandstein. M: Facies Muschelkalk. K: Facies Keuper. RG: Grupo Renales, comprende de base a techo las siguientes formaciones; Dolomías tableadas de Imón, Carniolas de Cortes de Tajuña y Calizas y dolomías tableadas de Cuevas Labradas. AG: Grupo Ablanquejo, comprende de base a techo las siguientes formaciones; Margas grises del Cerro del Pez, Calizas bioclásticas de Barahona y Alternancias de Margas y calizas de Turmiel. CH: Formaciones Carbonatos de Chelva y Margas de Sot de Chera. HV: Formaciones Huerteles y Valdeprado. T: Formaciones Aldealpozo y Torrecilla. SM: Formación Sierra Matute. OG: Grupo Oncala, comprende de base a techo las siguientes formaciones; Sierra Matute, Huerteles and Valdeprado. ML: Formación Malacara A: Formación Abejar. U: Facies «Utrillas». P: Formaciones Stª María de las Hoyas, Picofrentes y Muñecas. SD: Formaciones Hortezuelas, Hontoria del Pinar, Burgo de Osma, Santo Domingo de Silos y Santibáñez del Val. PG: Paleogeno. N: Neogeno.

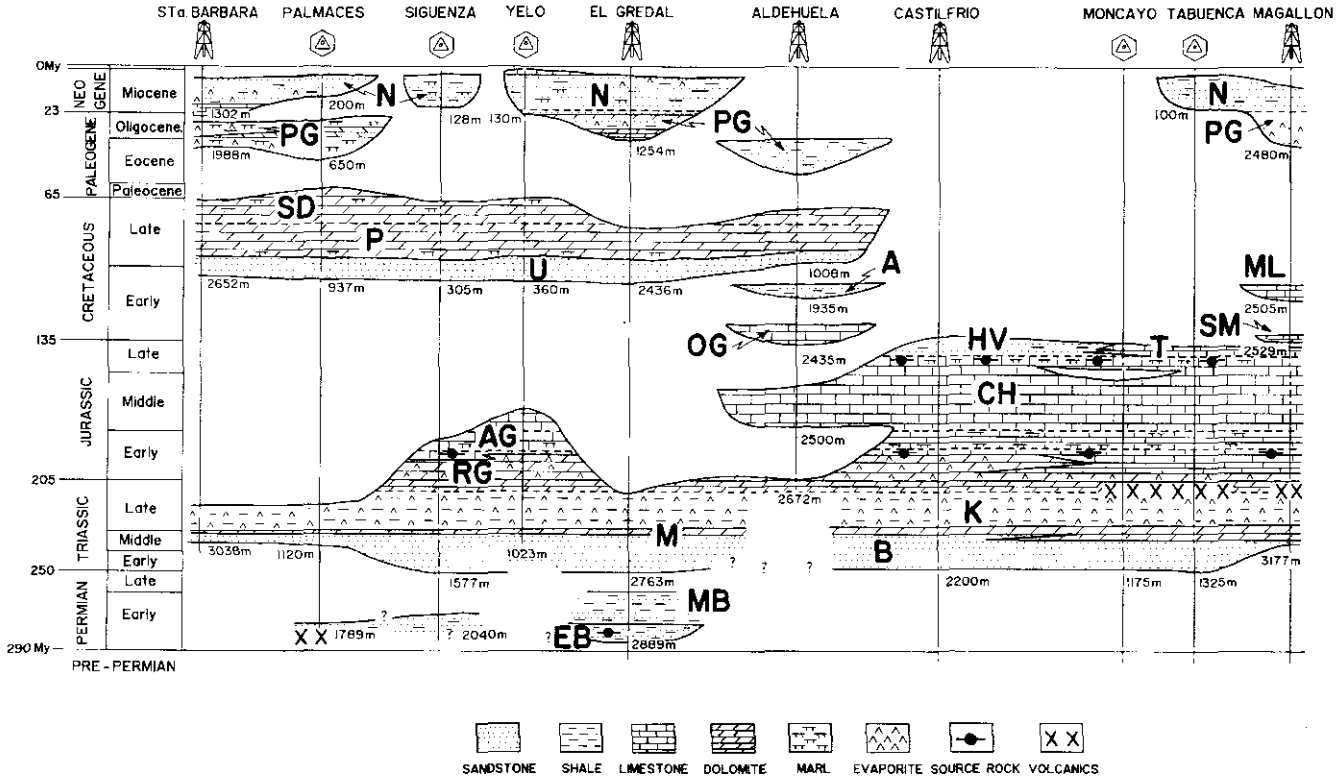
STa. BARBARA
PALMACES
SIGUENZA
YELO
EL GREDAL
ALDEHUELA
CASTILFRIO
MONCAYO
TABUENCA
MAGALLON
0My
23
65
135
205
250
290 My
NEO GENE
PALEOGENE
CRETACEOUS
JURASSIC
TRIASSIC
PERMIAN
Miocene
Oligocene
Eocene
Paleocene
Late
Early
Middle
Late
Middle
Early
Late
Early
PRE - PERMIAN
N
PG
SD
P
U
A
OG
HV
T
SM
ML
CH
AG
RG
M
K
B
MB
EB
1302m
200m
1988m
650m
128m
130m
1254m
100m
2480m
2652m
937m
305m
360m
2436m
1008m
1935m
2435m
2505m
2529m
2500m
2672m
3038m
1120m
1023m
1577m
2763m
2200m
1175m
1325m
3177m
1789m
2040m
2869m
SANDSTONE
SHALE
LIMESTONE
DOLOMITE
MARL
EVAPORITE
SOURCE ROCK
VOLCANICS

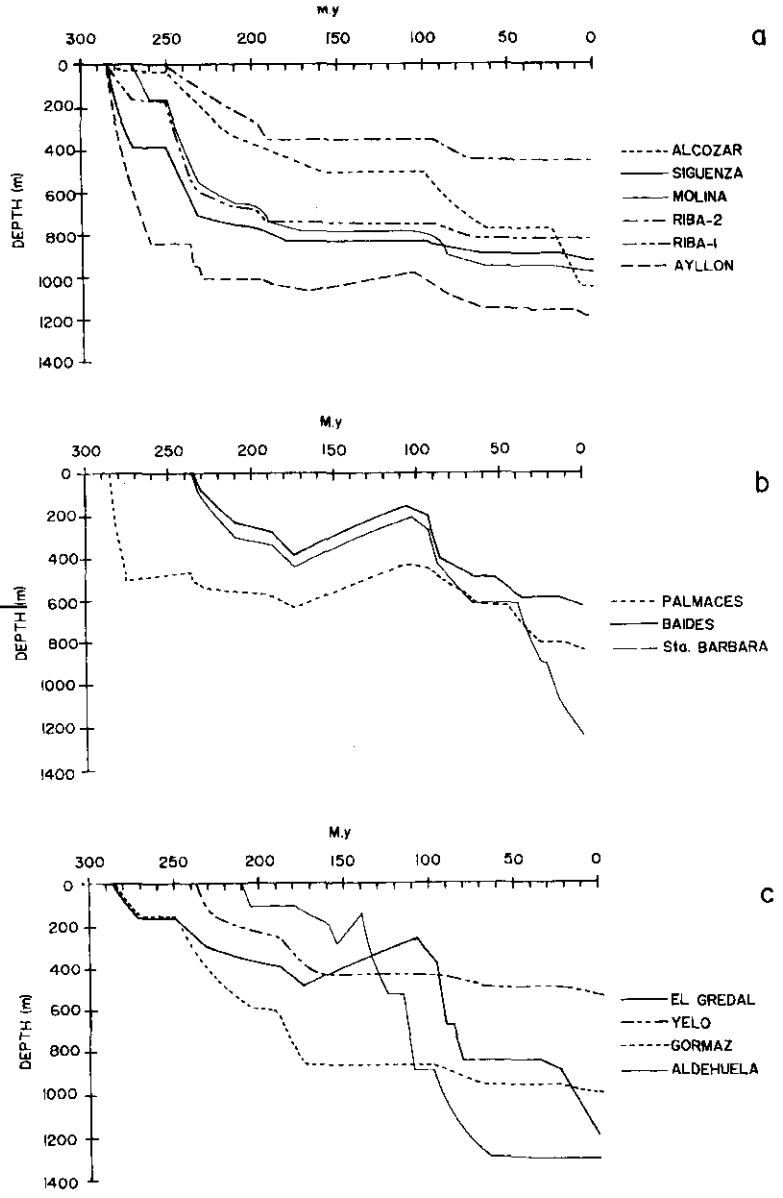

Figure 4.—Water loaded tectonic subsidence curves. For wells and dummy wells location see figure 2.

Figura 4.—Curvas de subsidencia tectónica. Localización de los sondeos y columnas de campo en figura 2.

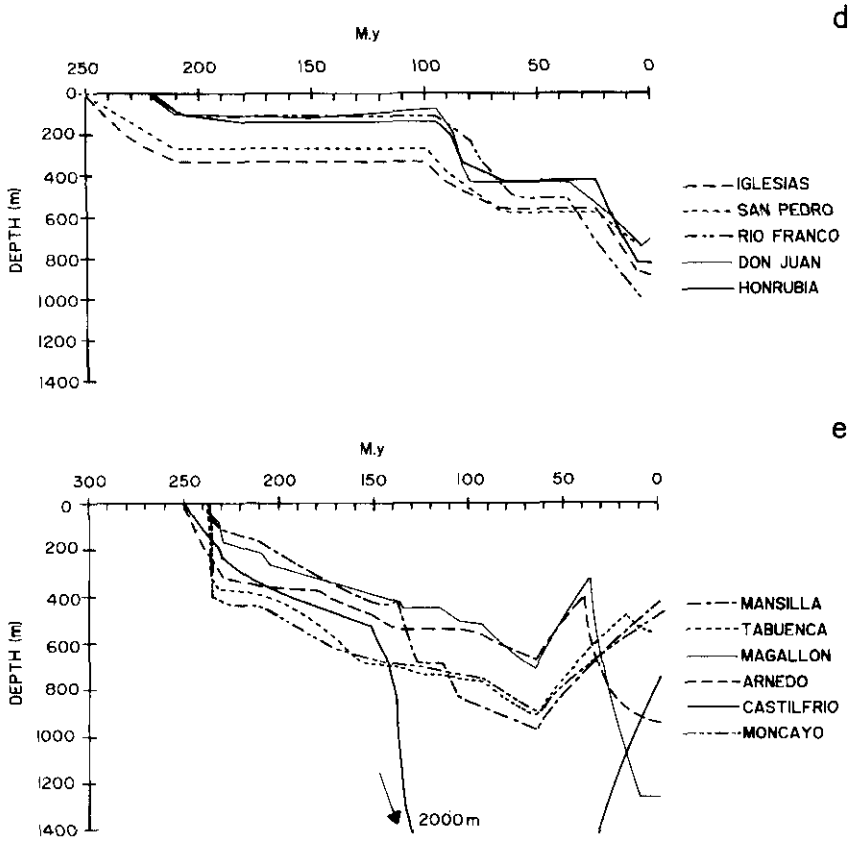

Figure 4.—Continue.
Figura 4.—Continuación.

The water-loaded tectonic subsidence history shows a similar form in all diagrams (fig. 4) but timing of rifting displays a propagation of extension with time. Considering the variations in age of the rifting onset, three successive «rifting/uplift realms» are defined (fig. 5b). First of all a Central Realm developed (C.R. in fig. 5b). This realm occupied an area similar to the previous Permian rift/uplift period. The rift/uplift area enlarged afterwards towards the East-North (Northeastern Realm, NE.R. in fig. 5b). During the third stage of evolution the rift/uplift covered the whole of the studied area affecting to the south-western area (south-western Realm, S.R. in fig. 5b). The limit of this realm is located at the margin of the cratonic basement where an unsedimented area is noted.

A structural cross-section through the area showing basement reconstruction and relationship resulting from the second stage of rifting /uplift (Permian and Triassic) is illustrated in Figure 6.

A third stage of rifting/uplift occurred during the Jurassic (≃ 205 to ≃ 140 My). Two realms based on backstripped subsidence curves are noted for this third rift/uplift period (fig. 7a) and an area of non-deposition and erosion has been distinguished. The two realms (Central C. R and North-eastern, NE. R in fig. 7a) show a progressive Eastern-Northern basin development. In the Central realm the subsidence again increased during the early Jurassic to Callovian (≃ 205 to ≃160 My) at relative low rates (fig. 4a, c) coupled with the dominance of carbonate over siliciclastic sediments. This subsidence episode was followed by a period of uplift and erosion during late Jurassic, recorded as trending upward segments on the tectonic subsidence curves (fig. 4b). In the Northeaster Realm (NE. R in fig. 7a) the age of rifting/uplift is younger (fig. 4e) than in the Central realm (fig. 4a, c). The subsidence episode continued until the Kimmeridgian (≃139 My) followed by a short trend towards uplift during the latest Jurassic. The almost zero subsidence history curves recorded in rest of the area (fig. 7a) for this stage (170 to 100 My) was probably due to epirogenic activity causing a period of erosion and possibly non-deposition. As a result of this evolution, the late Cretaceous siliciclastic sediments in this realm rest disconformably on Middle Palaeozoic rocks or paraconformably on late Triassic.

The Jurassic subsidence history, was probably a result of orthogonal opening of Central Atlantic, floor spreading of the Bay of Biscay, and sinistral translation between Africa and Europe, coupled with a relative sea level rise. The uplift episode was probably related with the late Kimmerian orogenic phase.

A fourth stage of rifting/uplift coupled with large sea level changes took place from the latest Jurassic through Middle Cretaceous (≃ 140 to ≃ 95 My). Only two realms, North-eastern (NE. R) and South-western (C-S. R), have been distinguished (fig. 7b) for the latest Jurassic-Middle Cretaceous rifting/uplift episode. In the North-eastern realm (NE.R in fig. 7b) a moderate initial episode of subsidence is recorded as a trending downward (fig. 4e) on the water loaded tectonic subsidence curves between ≃ 140 and ≃ 130 My. This is followed by uplift during late Berriasian through Middle Barremian. In the South-western realm (C-S. R. in fig. 7b) only the uplift episode is recorded on the curves. This episode was developed until Middle Albian (Austrian orogenic phase). In the North-eastern realm (fig. 4c), backstripped subsidence curves show a re-established subsidence regime towards the end of Barremian (≃ 114 My). This regime did not reach the South-western realm (fig. 4a, b, c and d) before Middle-late Albian (≃100 My).

From here (late Albian) onwards the backstripping curves show a major complexity as they are influenced not only by eustatic changes but also by the

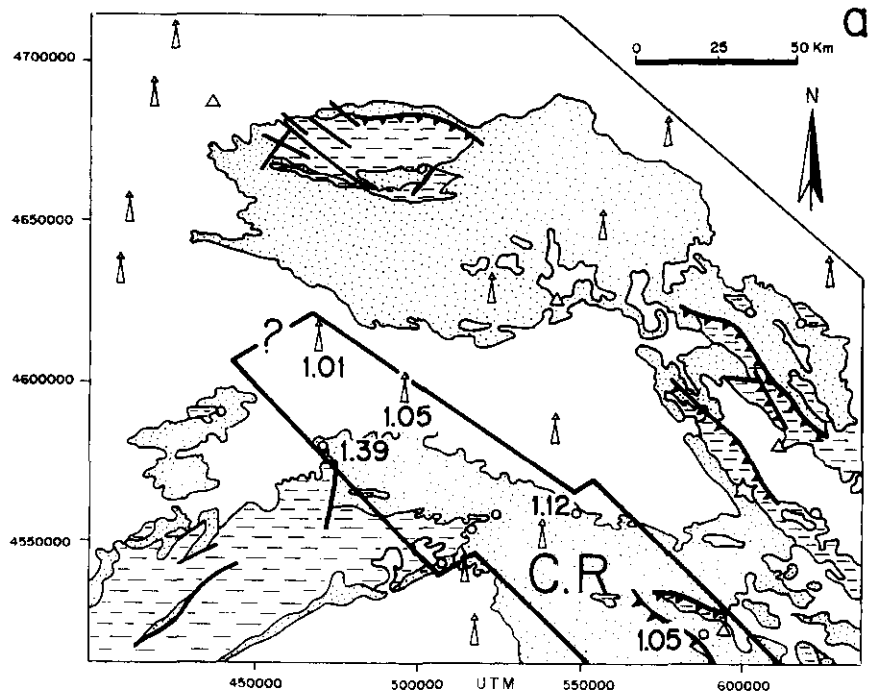

Figure 5a.—Rift/uplift realms determined for the Permian and stretching estimates (β) inferred from subsidence analysis. C.R.: central realm.
Figura 5a.—Dominios de extensión/elevación para el Pérmico y valor estimado del parámetro de extensión (β) a partir de las curvas de subsidencia tectónica. C.R.: dominio centro.

main compressional phases of Alpine orogeny. Compressional intraplate tangential stress can cause positive and negative lithospheric deflections which can be recorded in the curves. Therefore, this study has not included «rift/uplift realms» for those stages.

The subsidence history of the study area shows a general downwards trend from Middle-late Albian to the end of Cretaceous. This general increase in the subsidence rate was probably a response to both tectonic and an apparent rise in eustatic sea level (Haq, Hardenbol & Vail, 1987) that allowed an increase in accommodation space. As a result of these events a shallow marine carbonate environment was established during the early Cretaceous. This sedimentary regime was broken by siliciclastic dominantly non-marine sediments during late Aptian-Albian. The sea level rise during late Cretaceous generated a shifting of the sedimentary environments enabling allowing the development of a carbonate marine environment.

The Paleocene and Eocene tectonic subsidence curves show two trends. A tectonic uplift episode (≃ 65 My to ≃ 35 My), is recorded in figure 4e. Re-

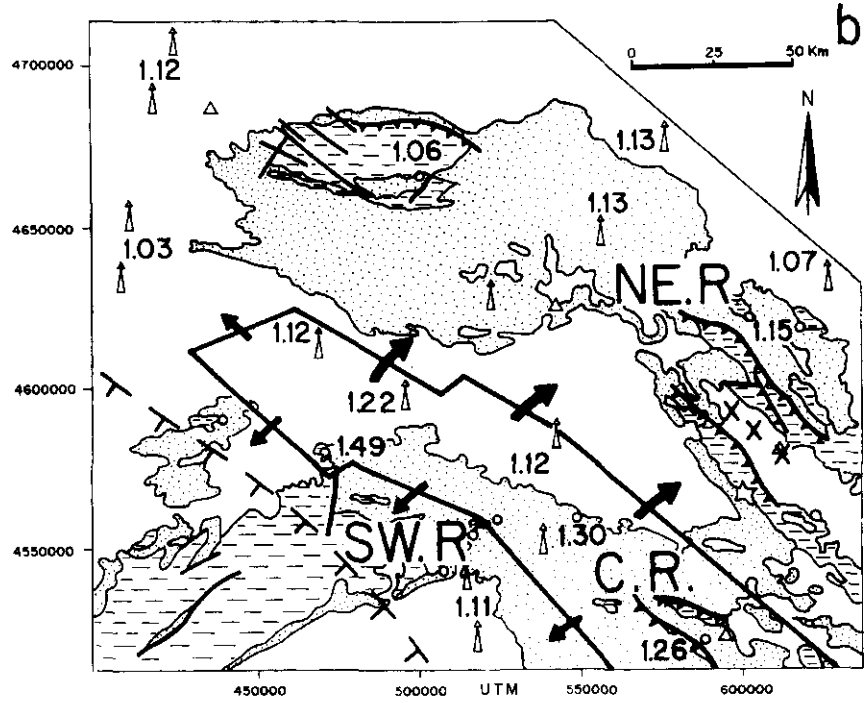

Figure 5b.—Rift/uplift realms determined for the Triassic and stretching estimates (β) inferred from subsidence analysis. SW. R: south-western realm. C.R.: central realm. NE. R.: north-eastern realm. Dashed lines with vertical strokes; non-triassic sedimentation recorded. Cross lines define the approximate locations of structural threshold. Note the sequence of overall propagation of activity and a gradual increase of stretching factor to the north-eastern (big arrows) and the south-western younging propagation (little arrows).

Figura 5b.—Dominios de extensión/elevación para el Triásico y valor estimado del parámetro de extensión (β) a partir de las curvas de subsidencia tectónica. SW. R: dominio sudoeste. C.R.: dominio centro. NE. R.: dominio noreste. Líneas discontinuas con trazos verticales; área sin registro de sedimentación triásica. La línea de cruces define la localización aproximada de los altos estructurales. La propagación de la actividad tectónica y el incremento en el valor del factor de extensión esta indicado por las flechas. La extensión inicialmente se propaga hacia el noreste (flechas de gran tamaño) y posteriormente hacia el sudoeste (flechas de pequeño tamaño).

maining curves display for this time horizontal segments that represent non-deposition and/or erosion (fig. 4a, b, c and d). Local anomalous pattern (fig. 4b) characterised by a continued downward-trending segment are due probably to sediment loading effects.

The tectonic subsidence history shows largely similar trends for the Oligocene, but wells located to the extreme east, (fig. 4e) and to the South (fig. 4d) display anomalous patterns characterised by a moderate subsidence episode.

The Miocene and Pliocene are depicted on water-loaded subsidence curves in a similar way (fig. 4) but not only the extreme areas show curves with downward-trending segments.

The overall pattern of tectonic subsidence observed during Paleogene is the result of Alpine compressional tectonic, Laramide and Pyrenean phases, whereas Neogene tectonic subsidence pattern is a result of Post-Alpine extensional stage.

Partial studies concerning subsidence analysis in Central Spain identified several stages of tectonic subsidence (Sanchez-Moya *et al.,* 1992; Salas & Casas, 1993; Roca, Guimera & Salas, 1994) which can be correlated with this study.

MATURITY MODELLING

Possible Source Rock

An accurate analysis of the characteristics of the different depositional units in the study area, has shown that three of them are the most propitious to be considered as source rocks: *Capas de la Ermita* Formation (Autunian), *Calizas y dolomías tableadas de Cuevas Labradas* Formation (Hettangian-Sinemurian) and *Margas de Sot de Chera* Formation (Oxfordian-Kimmeridgian) and their lateral equivalents (fig. 3).

No information about total organic content (TOC) is available from *Margas de Sot de Chera* Formation (Gomez & Goy, 1979) and the *Calizas y dolomías tableadas de Cuevas Labradas* Formation (Goy *et al.,* 1976). Margas de Sot de Chera Formation consist of grey marls with occasional limestone intercalation. Thickness ranges between 80 to 140 m. *Calizas y dolomias tableadas de Cuevas Labradas* consist of 50-150 m of shallow marine limestones and dolostones.

Two hypotheses on the total organic content were modelled: firstable a content of 1% TOC; second a content of 0.5 % TOC, probably a more realistic value. A type II kerogen (Tissot *et al.,* 1987) and the 10% by volume of the total formation as effective thickness was used in both cases. The accumulated thickness of organic-rich sediments in the interval is here considered as the effective thickness.

Early Permian potential source rocks correspond to *Capas de la Ermita* Formation (Sacher, 1966). Their distribution is irregular with a thickness of more than 300 m. This unit consists of three intervals (Ramos, 1979): volcanoclastics, lacustrine deposits (dark mudstones) and a dolomitic interval at the top. The effective thickness was the total thickness of the dark mudstones interval, and a type III kerogen was used.

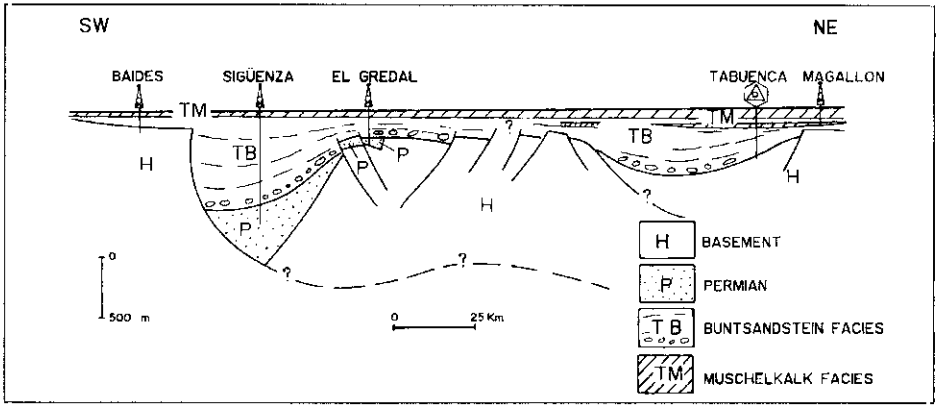

Figure 6.—Structural and stratigraphic cross-section trough the SW to the NE of the studied area for the Permian and Triassic based on well data, field sections and seismic data.
Figura 6.—Sección estructural y estratigráfica del área estudiada según un perfil SW-NE en base a los datos de sondeo, columnas de campo y sísmica disponible.

Determination of the organic matter content of Permian dark mudstones was evaluated from gamma-ray logs method (Schmoker, 1981) and formation-density logs methods by Schmorker (1979) and Myers & Jenkyns (1992). The TOC obtained was 0.39% using the gamma-ray method and 0.16% using the denstity log method. However, the accuracy of these methods is low due to the low quality and quantity of density logs in the studied area. The same as for Jurassic source rocks, and a content of 0.5% and 1% TOC was finally modelled.

Temperature Regime and Maturation

The degree and timing of thermal maturation of the rocks in the area can be evaluated with a steady-state thermal model and vitrinite reflectance history.

Neither specific nor general information on the present heat flow values and heat flow distribution in the study area was available. Therefore present day thermal distribution has been modelled using corrected bore-hole temperatures from 14 wells (and formation temperature logs when available) and a regional geothermal gradient of 3,1° C/100 m. The present day mean annual surface temperature has been taken in account too.

The present heat flow values were calculated using present geothermal gradient and rock thermal conductivities. Thermal conductivity values used in the models vary through time, depending on temperature and porosity re-

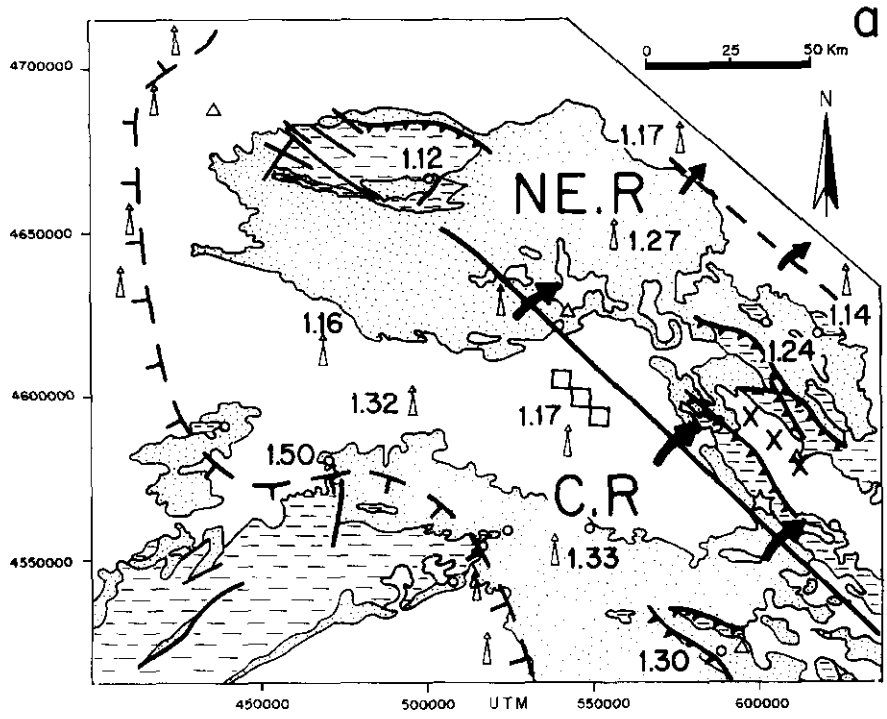

Figure 7a.—Rift/uplift realms determined for the Jurassic and stretching estimates (β) inferred from subsidence analysis. C.R.: central realm. NE. R.: north-eastern realm. Dashed lines with vertical strokes; non Jurassic sedimentation recorded. Cross line define the approximate locations of structural threshold. Diamonds line define a local high. Note the overall propagation of activity to the North-eastern (big arrows) and a second propagation event (little arrows) determine a «subrealm» in the same direction (dashed line).

Figura 7a.—Dominios de extensión/elevación para el Jurásico y valor estimado del parámetro de extensión (β) a partir de las curvas de subsidencia tectónica. C.R.: dominio centro. NE. R.: dominio noreste. Líneas discontinuas con trazos verticales; área sin registro de sedimentación jurásica. La línea de cruces define la localización aproximada de los altos estructurales. La línea de rombos define la localización de un umbral local. La propagación de la actividad tectónica y el incremento en el valor del factor de extensión esta indicado por las flechas. La extensión inicialmente se propaga hacia el noreste (flechas de gran tamaño) y posteriormente hacia el sudoeste (flechas de pequeño tamaño) definiendo un subdominio limitado por una línea discontinua.

duction corrections. Given the uncertainties surrounding conductivity and geothermal gradient, the interpretation of the results obtained has to be treated carefully.

Two different hypothesis have been modelled in this work: 1) a constant heat flow regime. 2) a rifting heat flow regime

In the first model, a constant heat flow regime of 40 mW/m^2, which is the global average heat flow value was used. The estimated present heat flow

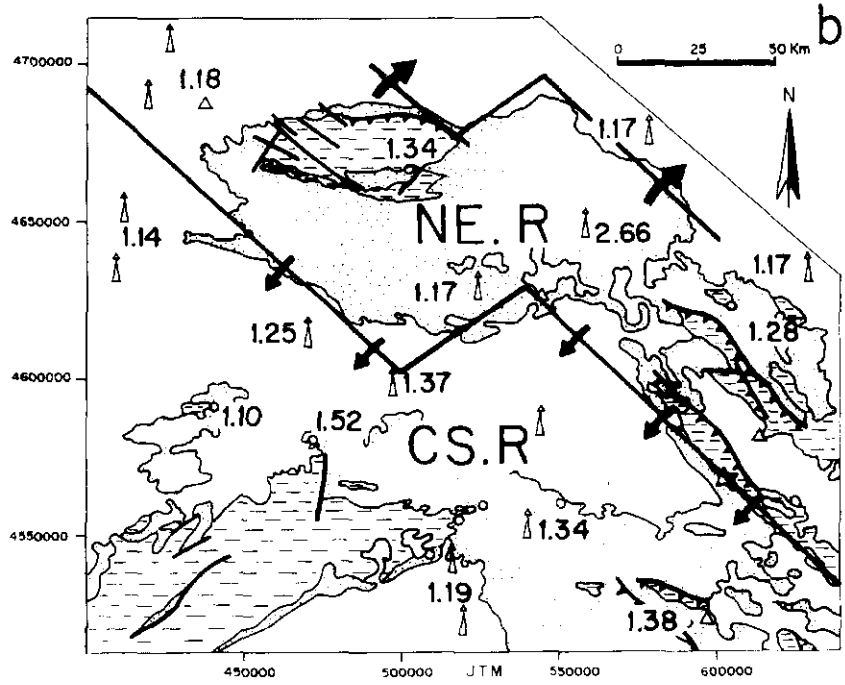

Figure 7b.—Rift/uplift realms determined for the Latest Jurassic though Middle Cretaceous and stretching estimates (β) inferred from subsidence analysis. CS.R.: south-western realm. NE. R.: *north-eastern realm. Note the sequence of overall propagation of activity to the north-eastern* (big arrows) and the south-western younging propagation (little arrows).
Figura 7b.—Dominios de extensión/elevación para el Jurásico superior-Cretácico medio y valor estimado del parámetro de extensión (β) a partir de las curvas de subsidencia tectónica. CS.R.: *dominio sodoeste. NE. R.: dominio noreste. La extensión inicialmente se propaga hacia el no*reste (flechas de gran tamaño) y posteriormente hacia el sudoeste (flechas de pequeño tamaño).

yields between 34 to 58 mW/m^2, when present day thermal data were used to calibrate present day bottom heat flow. This variability in the estimated present heat flow, may has been caused not only by differences in the types and qualities of present day thermal data, but also by differences in the tectonic evolution among between areas. An estimation of the present average heat flow of 43 mW/m^2, resulted when calibration was done. An average heat flow of 59.5 mW/m^2 resulted when only thermal history data were used to compute the present day bottom heat flow. Using an invariant paleothermal regime of 55 mW/m^2, a compute present average heat flow of 73.5 mW/m^2 were obtained. All values are conceivable and fall within the range obtained in specific heat flow studies in similar tectonic context (Lewis & Hymdman 1976; Mckenzie *et al.*, 1985; Issler & Beaumont, 1986 & 1987; Ritter 1987; Forbes

et al., 1991). It has to be emphasised that the calibrate average heat flow of 43 mW/m^2, that is the more realistic value, is very close to present average heat flow from eastern Canada passive margin (Hamdani & Mareschal, 1993)

The thermal history was subsequently modelled from subsidence data (rifting heat flow history). In a preliminary step, an estimation of crustal extension from a comparison of backstripped subsidence curves and tectonic subsidence predicted by stretching models (Mckenzie, 1978; Royden and Keen, 1980) was obtained. A simple one-layer stretching model of Mckenzie (1978) with instantaneous uniform stretching phases, according to rifting episodes fixed previously, has been used to determine β (crustal stretching factor) values.

The crustal stretching factor was obtained from direct comparison between backstripped subsidence curves performed and McKenzie (1978) theoretical tectonic subsidence curves.

The crustal stretching factors for every each rifting episode and «rift/uplift realm» are the numbers shown in figs. 5 and 7.

In the second modelled hypothesis a rifting heat flow regime was used. This paleothermal reconstruction computes a linear increase of the heat flow during rifting (Mckenzie 1978). It was assumed that the post-rifting heat flow would decrease accordingly to the Mckenzie Thermodynamic Model (Mckenzie, 1978).

The relationships between tectonic subsidence rate and heat flow, calculated for the most characteristic wells, show fluctuations and disagreement between tectonic subsidence rate and stretching heat flow. This is probably caused by uncertainties in backstripping and/or determination of the stretching factor. The lithospheric stretching modelling using a two-layer stretching model (Royden & Keen, 1980; Hellinger & Sclater, 1983) has to be done to allow a better understanding of the basin.

Vitrinite reflectance variations through time and depth were modelled with a correlation curve between reflectance and the modelled Transformation Ratio (TR). It represents the percentage of transformable organic matter converted into hydrocarbons at a given maturity stage, of the IFP (Institut Francais du Petrole) standard type III kerogen.

When rifting heat flow regime was used, the vitrinite reflectance values are below 0.4% R_0 for Permian or Jurassic source rocks. Values of 0.56% R_0 at 2814 m from Permian source rock in Ayllon, and of 0.5% R_0 at 1690 m in Castilfrio well, were exceptionally obtained.

The vitrinite reflectance values calculated using a constant HF = 40 mW/m^2 paleothermal heat flow and calibrated with present-thermal data are below 0.45% R_0 for Hettangian-Sinemurian source rock. For Oxfordian-Kimmeridgian source rocks, vitrinite reflectance reached a maximum value of 0.79% R_0 at 1690 m in Castilfrio well. Permian vitrinite reflectance values yield in the 0.43%-0.56% R_0 range reached at 1800 and 2814 m in both Ribal and Ayllon.

Assuming a constant paleo-thermal heat flow (HF= 40 mW/m^2 and HF= 55 mW/m^2), without calibration, the vitrinite reflectance values obtained were slightly larger than values computed with the preceding terms. The vitrinite reflectance values (R_0), Transformation Ratio (TR), Hydrocarbon Index (HI) and Temperature of Peak Petroleum Generation (Tmax), obtained using a total organic content of 1% TOC from Jurassic and Permian source rocks as shown in Table II.

Hydrocarbon generation history

As discussed before, to simulate the history of kerogen degradation, hydrocarbon generation history and the type and amount of hydrocarbons generated, a set of kinetic equations (Tissot & Espitalié, 1975 ; Tissot *et al.* 1987; Quigley, MacKenzie & Gray, 1987; Espitalié *et al.*, 1988; Burnhan & Braun, 1990; Ungerer *et al.*, 1990; Castelli *et al.*, 1990) and a set of default kinetic parameters (Evans & Felbeck, 1983; Espitalié *et al.*, 1988; Forbes *et al.*, 1991) were used.

The classical vitrinite reflectance threshold (Tissot & Welte, 1984) was the default used to define maturity windows.

The results of calculating oil and gas generation in the study area, assuming a paleothermal constant regime HF=40 mW/m^2 without calibration is shown in Table III.

The results of modelling Rock-Eval indicate that Permian source rocks are mature in Ayllon, (top of the mature zone at 2054 m), partially mature in Sigüenza, Molina, Gormaz and Alcozar (see fig. 2 for location) and immature in the rest of the wells. Hettangian to Senonian source rocks are immature. The late Jurassic (Oxfordian-Kimmeridgian) are mature in Aldehuela (top of the mature zone al 2203 m) and overmature in Castilfrio (tables II and III).

A maximum hydrocarbon generation from Permian source rocks is recorded at Ayllon with a value of 0.55 mgHC/gTOC. A generation close to 4 mgHC/gTOC was computed in Gormaz from Hettangian-Sinemurian source rock. Only very minor hydrocarbon generation about 6.56 mgHC/gTOC (tables II and III) has occurred in Oxfordian-Kimmeridgian source rocks at Castilfrio well (maximum value).

Evaluation of the study area is initially unfavourable based on the discussion above.

CONCLUSIONS

A general picture of subsidence, thermal and hydrocarbon generation histories of the study area has been developed using a one-dimensional, single-well, model. However, backstripping and maturation modelling were useful,

HF = 40mW/m²				Locations	Source rock Kerogen type	HF = 55mW/m²			
$\%R_0$	%TR	HI mg/g	Tmax °C			$\%R_0$	%TR	HI mg/g	Tmax °C
0.58	0.2	224	442	Alcozar	P-Type III	0.76	4.3	224	442
0.83		225	442	Aldehuela	Ord/Kim-Type II	1.32		225	443
0.46	1.4	652	416	Arnedo	Het/Sin-Type II	0.55	3.5	638	416
0.85	9.5	203	444	Ayllon	P-Type III	1.34	62.3	84	467
		661	416		Het/Sin-Type II		0.1	661	416
		225	444	Baides	Het/Sin-Type II	0.45		225	467
2.36	99	6	550	Castilfrio	Oxf/Kim-Type II	3.79	100.0	0	585
0.58	0.4	224	442	Gormaz	P-Type III	0.73	3.1	218	443
	0.6	657	416		Het/Sin-Type II	0.45	1.2	654	416
0.56	0.3	224	442	El Gredal	P-Type III	0.71	2.7	219	443
0.49		225	548		Het/Sin-Type II	0.60		225	585
0.46	1.4	653	416	Honrubia	Het/Sin-Type II	0.54	3.5	638	416
0.57	4.8	630	417	Magallon	Het/Sin-Type II	0.73	3.4	436	420
0.59	0.5	224	442	Molina	P-Type III	0.75	4.1	215	443
	0.1	661	416		Het/Sin-Type II		0.5	658	416
	0.4	659	416	Moncayo	Het/Sin-Type II	0.44	1.0	655	416
0.51		225	442	Palmaces	P-Type III	0.61	0.7	221	442
0.53	0.1	225	442	Riba-1	P-Type III	0.63	0.9	223	442
		661	416		Het/Sin-Type II			661	416
		661	416	Riba-2	Het/Sin-Type II			661	416
0.59	0.5	224	442	Sigüenza	P-Type III	0.74	3.7	216	443
		661	416		Het/Sin-Type II			661	416
0.42	0.8	656	416	Tabuenca	Het/Sin-Type II	0.47	1.6	651	416
		661	416	Yelo	Het/Sin-Type II		0.1	661	416

Table II.—Vitrinite reflectance (R_0), transformation ratios of kerogen to petroleum (TR), hydrogen index (HI), and temperature of peak petroleum generation (Tmax.) achieved from heat flow modelled (HF = 40mW/m² and HF = 55mW/m²) and kerogen type for source rock formations.

Tabla II.—Valores de la reflectividad de la vitrinita (Ro), tasa de transformación del kerogeno a petróleo (TR), índice de hidrogeno (HI) y temperatura de generación del petróleo (Tmax.) obtenidos por modelización para las rocas madre consideradas y distintos valores del flujo de calor (HF = 40mW/m² y HF = 55mW/m²).

HF = 40mW/m²				Locations	Kerogen type	HF = 55mW/m²			
C6+	Gas	Coke	GOR			C6+	Gas	Coke	GOR
mg HC/g dry roc			m^3/m^3			mg HC/g dry roc			m^3/m^3
0.19			0.94	Alcozar	Type III-P	0.26	0.01		36.0
0.44			0.18	Arnedo	Type II-J_1	0.56	0.1		18.0
0.35	0.2		82.0	Ayllon	Type III	1.24	0.2	0.03	190.0
0.35			$1.3\ 10^3$	Type II-J_1	0.36			0.11	
	3.27	3.29		Castilfrio	Type II-J_3		3.32	3.29	
0.19			0.65	Gormaz	Type III-P	0.24			22.0
3.90			0.32		Type II-J_1	4.22			0.96
0.19			0.42	El Gredal	Type II-P	0.23			18.0
					Type III-J_1				
0.43			1.6	Honrubia	Type II-J_1	0.56	0.01		18.0
0.64	0.1		24.0	Magallón	Type II-J_1	241	0.08		37.0
0.19			0.97	Molina	Type III-P	0.26	0.1		34.0
0.35			0.013		Type II-J_1	0.38			0.075
0.38			0.059	Moncayo	Type II-J_1	0.41			0.48
0.35			$1.6\ 10^{-3}$		Type II-J_3	0.36			0.016
0.18			0.051	Palmaces	Type III-P	0.19			16.0
0.18			0.082	Riba-1	Type III-P	0.10			2.5
0.35			$7.6\ 10^{-4}$		Type II-J_1	0.35			$2.5\ 10^{-3}$
0.19			0.86	Sigüenza	Type III-P	0.25	0.01		28.0
0.35			$8.2\ 10^{-4}$		Type II-J_1	0.35			$2.7\ 10^{-3}$
0.40			0.25	Tabuenca	Type II-J_1	0.45			25.0
0.35			$2.2\ 10^3$	Yelo	Type II-J_1	0.36			$9\ 10^{-3}$

Table III.—Total generated quantity for each HC fraction (C6+, gas and coke) and the total gas/oil ratio (GOR) achieved from heat flow modelled (HF = 40mW/m² and HF = 55mW/m²) and kerogen type for source rock formations.

Tabla III.—Estimación de la cantidad total de hidrocarburos generados (petróleo, gas y carbón) y relación gas/petróleo (GOR) obtenidos por modelización para las rocas madre consideradas y distintos valores del flujo de calor (HF = 40mW/m² y HF = 55mW/m²).

not only to determine and extend maturation results to sparse investigated and/or undrilled parts in the study area, but also to reconstruct the tectonic and thermal evolution of the basin.

The tectonic subsidence record focuses on the structure of the study area and reflects differential movements of separate basement blocks during early Alpine to late Alpine tectonic evolution. The differences between interpreted basement behaviour recorded in tectonic subsidence curves by each rift/uplift stage permitted four major «rift/uplift realms» to be distinguished. The tectonic subsidence history is summarised in fig. 4.

A first stage of rift/uplift occurred during late Permian. This extensional episode resulted in the formation of a complex system of small and isolated NW-SE trending half grabens filled by hundreds of meters of red beds during late Permian (Sopeña *et al.,* 1988). This period of subsidence was followed by a period of uplift and erosion. Only one realm (Central Realm) shows extensional processes (fig. 5a).

A second stage of rifting/uplift took place during Triassic. A subsidence peak took place during deposition of Buntsandstein facies to Muschelkalk facies, followed by a pseudo-exponential late Triassic subsidence. A propagation of extension with time, can be observed and three «realms» are defined (fig. 5b); Central, with an early record of tectonic subsidence and North-eastern and South-western that were affected by intraplate distensive regime. This rifting period can be related with the late Variscan to early Alpine stage on the Iberian Peninsula that might represent the initial break up of the central part of Pangea.

A third stage of rifting/uplift occurred in the Jurassic. The distinguished realms based on backstripped subsidence curves for this rift/uplift period (fig. 7a) display a progressive north-eastern south-western propagation in rifting/uplift. The Jurassic subsidence history, was probably a result of orthogonal opening of Central Atlantic, floor spreading of the Bay of Biscay, and sinistral translation between Africa and Europe, coupled with a relative sea level rise.

A fourth Mesozoic stage of rifting/uplift coupled with large sea level changes took place from the Latest Jurassic through Middle Cretaceous. The North-eastern realm was characterised by a moderate episode of subsidence (among 140 and 130 My). This episode was followed by uplift during late Berriasian through Middle Barremian. A re-establishment of subsidence regime towards the end of Barremian took place. Initial Cretaceous subsidence was not recorded in the rest of the study area and the uplift episode spanded until Middle Albian followed by a resumption on the tectonic subsidence from Middle-late Albian ($\simeq$ 100 My). The subsidence history of the study area shows a general downwards trend during Middle-late Albian to the end of Cretaceous, with minor subsidence pulses. This general increase in the subsidence rate was probably a response of both tectonic and an apparent rise in eustatic sea level.

The Paleocene and Eocene tectonic subsidence curves in the east area show another tectonic uplift episode. The curves of remaining areas, display for this time horizontal segments that represent non-deposition and/or erosion, with local anomalous pattern probably due to sediment loading effects. The Oligocene tectonic subsidence history shows a largely similar trend, characterised by a moderate subsidence episode. Miocene and Pliocene are depicted on water loaded subsidence curves in a similar way. The overall pattern of tectonic subsidence observed during Paleogene are the result of Alpine compressional tectonics, whereas Neogene tectonic subsidence pattern is a result of Post-Alpine extensional stage.

At a broad regional scale, the study area seems to have been divided into diverse areas affected by one or more intense rifting/uplift phases, that were separated by basement blocks of less-intense deformation. These «rift/uplift realms» show a propagation of rifting/uplift stages along time. The three prior episodes (Permian, Triassic and Jurassic) show an initial north-western propagation followed by a south-western propagation from the Central realm. Each of these realms shows also a gradual north-western progression of the extension strain. The Cretaceous rift/uplift stage seems to behave in the opposite direction.

Present day bottom heat flow and thermal history were modelled, with steady state thermal model and paleo thermal heat flow invariant. Calibration from present day thermal data and imposed heat flow history were used. The present average bottom heat flow obtained falls within the range of values reported in the literature among similar tectonic contexts. Subsequently rifting heat flow history was modelled, pointing out that non-uniform stretching model requires to be applied.

The predictive and accuracy ability of the models in hydrocarbon generation depends largely on the uncertainty of heat flow patterns. Therefore different heat flow values were tentatively adopted to determine maturation. All the quantitative estimations of generated hydrocarbons indicate that insignificant volumes of hydrocarbons were generated by source rocks considered in this study.

ACKNOWLEDGMENTS

This paper benefited greatly from the comments, suggestions, discussions and not published lithostratigraphic data received from Alvaro Garcia-Quintana .We thank Ramon Mas, J.J. Gomez Fernandez and J.C. Gomez-Fernandez for sharing unpublished data with us. Carlos Beroiz (Repsol, S.A.) is thanked for providing access to Matoil™, and for his constructive suggestions. Thanks are due to J.M. Gaulier (I.F.P.) and R. Tocco (INTEVEP, S.A.) for reading the original manuscript. Agustin Pieren are thanked for his careful review and helpful comments and contributions to the final text. This work is a contribution to the project PB94-1219 funded by the CICYT.

REFERENCES CITED

ADELL, F., GONZÁLEZ-LODEIRO, F. & TENA-DAVILA, F., (1981), *Mapa Geológico de España. E. 1:50.000, MAGNA,* Hoja núm. 461 (Sigüenza), Servicio de Publicaciones del Ministerio de Industria y Energía, Madrid, 57 pp.

ADELL, F., GONZÁLEZ-LODEIRO, F., TENA-DAVILA, M., GABALDÓN, V. & RUIZ, P. (1982), *Mapa Geológico de España. E. 1:50.000, MAGNA,* Hoja núm. 434 (Barahona), Servicio de Publicaciones del Ministerio de Industria y Energía, Madrid, 57 pp.

ADELL, F., LENDINEZ, A., MARTÍNEZ, F. & TENA-DAVILA, M. (1981), *Mapa Geológico de España. E. 1:50.000, MAGNA,* Hoja núm. 513 (Zaorejas), Servicio de Publicaciones del Ministerio de Industria y Energía, Madrid, 44 pp.

ALONSO, A., (1981), «El Cretácico de la provincia de Segovia (borde norte del Sistema Central)», *Seminar. Estratigr. Serie Monografías*, Editorial de la Universidad Complutense de Madrid, 7, 271 pp.

— FLOQUET, M., MELÉNDEZ, A. & SALOMÓN, J. (1982), «Cameros-Castilla», in *El Cretácico de España*. Dpto. Estratigrafía, (ed.). Universidad Complutense de Madrid, 345-387.

ALONSO GAVILÁN, G., ARMENTEROS, I., DABRIO, C. & MEDIAVILLA, R. M. (1987), «Depósitos lacustres terciarios de la Cuenca del Duero (España)», *Stud. Geol. Salmant.*, 24 (Supl. 1), 47 pp.

ALVARO, M., CAPOTE, R. & VEGAS, R., (1979), «Un modelo de evolución geotectónica para la Cadena Celtiberica», *Acta Geol. Hisp.*, 14, 172-177.

ANCOCHEA, E., SAGREDO, J., MUÑOZ, M. & NAVIDAD, M. (1994), *El magmatismo Permo-Carbonífero de la Rama Oriental de la Cordillera Ibérica,* III Coloquio de Estratigrafía y Paleogeografía del Pérmico y Triásico de España. Resúmenes, Cuenca, España, 7-8

ARRIBAS, J. (1984), *Sedimentología y diagénesis del Buntsandstein y Muschelkalk de la Rama Aragonesa de la Cordillera Ibérica (Provincias de Soria y Zaragoza),* Tesis Doctoral, Universidad Complutense de Madrid (Inédita), 354 pp.

ARTHAUD, F. & MATTE, P. (1977), «Late Paleozoic strike-slip faulting in Southern Europe and North Africa; results of a right-lateral shear zone between the Appalachians and the Urals», *Geol. Soc. Am. Bull.*, 88, 1305-1320.

AURELL, M. (1990), *El Jurásico superior de la Cordillera Ibérica Central (Provincias de Zaragoza y Teruel). Análisis de Cuenca,* Tesis Doctoral, Universidad de Zaragoza (Inédita), 389 pp.

BARRÓN, E. & GOY, A. (1994), *Caracterización palinológica del tránsito Triásico-Jurásico en la Región de Sigüenza (Guadalajara, España),* III Coloquio de Estratigrafía y Paleogeografía del Pérmico y Triásico de España. Resúmenes, Cuenca, España, 13

BASCONES, L., LENDINEZ, A., MARTÍN, D. & TENA-DAVILA, M. (1981), *Mapa Geológico de España. E. 1:50.000, MAGNA,* Hoja núm. 514 (Taravilla), Servicio de Publicaciones del Ministerio de Industria y Energía, Madrid, 59 pp.

BURNHAM, A. K. & BRAUN, R. L., (1990), «Detailed model of petroleum formation, destruction and expulsion from lacustrine and marine source rocks», in *Advances in Organic Geochemistry*, Durand, B., and Behar, F., (eds.), Pergamon Press, Oxford, 16, 27-40.

CABALLERO, J. M., GONZÁLEZ-CASADO, J. M., CASQUET, C., GALINDO, C. & TORNOS,

F.(1996), «Episienitas de la Sierra de Guadarrama: un proceso hidrotermal regional de edad Pérmico inferior ligado al inicio de la extensión Alpina», *Cuad. Geol. Ibérica*, 20, 183-201.

CAPOTE, R., DÍAZ, M., GABALDÓN, V., GÓMEZ, J., SÁNCHEZ DE LA TORRE, L., RUIZ, P., ROSELL, J., SOPEÑA, A. & YEBENES, A. (1982), «Evolución sedimentológica y tectónica del ciclo Alpino en el tercio Noroccidental de la Rama Castellana de la Cordillera Ibérica», *Temas Geol. Min. Int. Geol. Min. España*, 5, 289 pp.

CASTELLI, A., CHIARAMONTE, M. A., BELTRAME, L., CARNITI, R., DEL BIANCO, A. & STROPPA, F. (1990), «Thermal degradation of kerogen by hydrous pyrolysis: a kinetic study», in *Advances in Organic Geochemistry*, Durand, B., and Behar, F. (eds.), Oxford, Pergamon Press, 16, 75-82.

CLEMENTE, P. & ALONSO, A. (1990), «Estratigrafía y sedimentología de las facies continentales del Cretácico inferior en el borde meridional de la Cuenca de los Cameros», *Estudios Geol.*, 46, 257-276.

DOBLAS, M., LÓPEZ-RUIZ, J., OYARZUN, R., MAHECHA, V., SÁNCHEZ-MOYA, Y., HOYOS, M., CEBRIÁ, J. M., CAPOTE, R., HERNÁNDEZ-ENRILE, J. L., LILLO, J., LUNAR, R., RAMOS, A. & SOPEÑA, A. (1994a), «Extensional tectonics in the Central Iberian Peninsula during the Variscan to Alpine transition», *Tectonophysics*, 238, 95-116.

DOBLAS, M., OYARZUN, R., SOPEÑA, A., LÓPEZ-RUIZ, J., CAPOTE, HERNÁNDEZ-ENRILE, J. L., HOYOS, M., LUNAR, R. & SÁNCHEZ-MOYA, Y. (1994b), «Variscan-late Variscan-early Alpine progressive extensional collapse of central Spain», *Geodinamica Acta*, 7, 1-14.

ESPITALIÉ, J., UNGERER, , IRWIN, I. & MARQUIS, F. (1988), «Primary craking of kerogens. Experiment and modelling C1,C2-C5, C6-C15 and C15+ classes of hydrocarbons formed», in *Avances in Organic Geochemistry*, Matavelli, L., and Novelli, L., (eds.), Pergamon Press, Oxford, 13, 893-899.

EVANS, R. J. & FELBECK, G. T. (1983), «High temperature simulation of petroleum formation-I. The pyrolysis of Green River shale», *Organic Geochemistry*, 4, 135-144.

FLOQUET, M., ALONSO, A. & MELÉNDEZ, A. (1982), «Cameros-Castilla: el Cretácico superior», in *El Cretácico de España*, Dpto. Estratigrafía, (ed.). Universidad Complutense de Madrid, 387-456.

FORBES, L., UNGERER, P. M., KUHFUSS, A. B., RIIS, F. & EGGEN, S. (1991), «Compositional modelling of petroleum generation and expulsion: Trial application to a local mass balance in the Smorburkk Sor Field, Haltembanken Area, Norway», *Amer. Assoc. Petrol. Geol. Bull.*, 75, 873-893.

GÓMEZ, J. J. & GOY, A. (1979), «Las Unidades Litoestratigráficas del Jurásico medio y superior en facies carbonatadas del sector levantino de la Cordillera Ibérica», *Estudios Geol.*, 35, 569-598.

GÓMEZ FERNÁNDEZ, J. C. (1992), *Análisis de la Cuenca sedimentaria de los Cameros durante sus etapas iniciales de relleno en relación con su evolución paleogeográfica*, Tesis Doctoral, Universidad Complutense de Madrid (Inédita), 343 pp.

GOY, A., GÓMEZ, J. & YEBENES, A. (1976), «El Jurásico de la Rama Castellana de la Cordillera Ibérica (Mitad Norte). I Unidades Litoestratigráficas», *Estudios Geol.*, 32, 391-423.

GOY, A. & MÁRQUEZ-ALIAGA, A. (1994), *Bivalvos norienses de la Formación Imon en Renales (Guadalajara, España)*, III Coloquio de Estratigrafía y Paleogeografía del Pérmico y Triásico de España. Resúmenes, España, 47-48.

GOY, A. & MARTÍNEZ, G. (1996), «Nautiloideos del Triásico medio en la Cordillera Ibérica y en la parte oriental de las Cordilleras Béticas», *Cuad. Geol. Ibérica,* 20, 271-300.

GOY, A. & YEBENES, A. (1977), «Características, Extensión y edad de la formación Dolomías tableadas de Imon», *Cuad. Geol. Ibérica*, 4, 375-384.

GUIRAUD, M. & SEGURET, M. (1985), «A releasing solitary overstep model for the Late Jurassic-Early Cretaceous (Wealdian) Soria strike-slip Basin (Northern Spain)», *Soc. Econ. Paleont. Mineral.* Spec. Publ., 37, 159-175.

HAMDANI, Y. & MARESCHAL, J. C. (1993), «Paleo heat flow of eastern Canada's passive margins», *Tectonophysics*, 225, 107-121.

HAQ, B. U., HARDENBOL, J., & VAIL, R. (1987), «Chronology of fluctuating sea levels since the Triassic», *Science*, 235, 1156-1167.

HELLINGER, S. & SCLATER, J. (1983), «Some comments on two-layer extensional models for the evolution of sedimentary basin», *Jour. Geophys. Res.*, 88, 8251-8270.

HERNANDO, S. (1977), «Pérmico y Triásico de la región Ayllon-Atienza (provincias de Segovia, Soria y Guadalajara)», *Seminar. Estratigr. Serie Monografías*, Editorial de la Universidad Complutense de Madrid, 2, 408 pp.

— & RINCÓN, R. (1987), «El Triásico del sector de Mansilla (Demanda Suroriental-La Rioja)», *Cuad. Geol. Ibérica*, 11, 691-706.

ISSLER, D. R. & BEAUMONT, C. (1986), «Estimates of terrestrial heat flow in offshore eastern Canada: Discussion», *Can. Jour. Earth Sci.*, 23, 2083-2085.

— (1987), «Thermal and subsidence history of the Labrador and West Greenland continental margins», in *Sedimentary basin and basin-forming mechanisms*, Beaumont, C. & Tankard, A. (eds.), *Can. Soc. Petrol. Geol. Mem.*, 12, 45-69.

LAGO, M., POCOVI, A., BASTIDA, J., ARRANZ, E., VAQUER, R. & DUMITRESCU, R. (1994), *Valor cronoestratigráfico del magmatismo alcalino, Triás-Lías, en la Cadena Ibérica, Cadena Costero-Catalana y Sierra Norte de Mallorca,* III Coloquio de Estratigrafía y Paleogeografía del Pérmico y Triásico de España. Resúmenes, Cuenca, España, 63-64.

LEWIS, J. F. & HYNDMAN, R. D. (1976), «Oceanic heat-flow measurements over the continental margins of eastern Canada», *Can. Jour. Earth Sci.*, 13, 1031-1038.

MACKENZIE, A. S., BEAUMONT, C., BOUTILIER, R. & RULLKÖTTER, J. (1985), «The aromatization and isomerization of hydrocarbons and the thermal and subsidence history of the Nova Scotia margin», *Phil. Trans. Roy. Ast. Soc. London*, 315, 203-232.

MACKENZIE, D. (1978), «Some remarks on the development of sedimentary basins», *Earth Planet. Sci. Letters,* 40, 25-32.

MUÑOZ, A. (1993), *Análisis del Pérmico y Tríasico en el subsuelo del tercio noroccidental de la Cordillera Ibérica y áreas adyacentes,* Tesis Doctoral, Universidad Complutense de Madrid (Inédita), 374 pp.

MYERS, K. J. & JENKYNS, K. F. (1992), «Determining total organic carbon contents from well logs: an intercomparison of GST data & a new density method», in *Geological Applications of wireline logs II*, Hurst, A., Griffiths, C. M. & Worthington, F., (eds.), *Geol. Soc. London Spec.Pub.*, 65, 369-376.

NELSON, R. A., PATTON, T. L. & MORLEY, C. K. (1992), «Rift-Segment interaction and its relations to hydrocarbon exploration in continental rift systems», *Amer. Assoc. Petrol. Geol. Bull.*, 76, 1153-1169.

PÉREZ MAZARIO, F. (1990), «Depósitos de abanicos aluviales distales en la unidad inferior del Pérmico del borde noreste del Sistema Central», *Geogaceta*, 8, 69-70.

PERRIER, R. & QUIBLIER, S. (1974), «Thickness changes in sedimentary layers during compaction history», *Amer. Assoc. Petrol. Geol. Bull.*, 58, 507-520.

POCOVI, A., LAGO, M. & BASTIDA, J. (1988), *Características del emplazamiento del magmatismo alcalino del transito Trías-Lías de la Cadena Ibérica,* III Coloquio de Estratigrafía y Paleogeografía del Jurásico de España. Comunicaciones, Logroño, España, 77-79.

QUIGLEY, T. M., MACKENZIE, A. S. & GRAY, J. R. (1987), «Kinetic theory of petroleum generation», in *Migration of Hydrocarbons in Sedimentary Basins*, Doligez, B., (ed.). Technip, Paris, 649-666.

QUINTERO, I., GÓMEZ, E., MANSILLA, H., MARTÍNEZ, C. & VILLENA, J.(1981), *Mapa Geológico de España. E. 1:50.000, MAGNA,* Hoja núm. 489 (Molina de Aragón), Servicio de Publicaciones del Ministerio de Industria y Energía, Madrid, 55 pp.

RAMOS, A. (1979), «Estratigrafía y Paleogeografía del Pérmico y Triásico del W de Molina de Aragón (prov. de Guadalajara)», *Seminar. Estratigr.*, Serie Monografías, 6, 313 pp.

— SOPEÑA, A. & PÉREZ-ARLUCEA, M. (1986), «Evolution of Buntsandstein fluvial sedimentation in the Northwest Iberian ranges (Central Spain)», *Jour. Sed. Petrol.*, 56, 862-875.

RITTER, U. (1987), «Modelling of hydrocarbon generation patterns in the Egersund Sub-Basin, North Sea», *Organic Geochemistry*, 13, 165-174.

ROCA, E., GUIMERA, J. & SALAS, R. (1994), «Mesozoic extensional tectonics in the Southeast Iberian Chain», *Geol. Mag.*, 131, 155-168.

ROYDEN, L. & KEEN, C. E. (1980), «Rifting process and thermal evolution of the continental margin of eastern Canada determined from subsidence curves», *Earth Planet. Sci. Letters*, 51, 343-361.

SACHER, L. (1966), «Stratigraphie und Tektonik der nord westlichen Hesperischen Ketten bei Molina de Aragón, Teil I Stratigraphie (Palaozoikum)», *N. Jb. Geol. Palaont. N.*, 124, 151-167.

SALAS, R. & CASAS, A. (1993), «Mesozoic extensional tectonics stratigraphy and crustal evolution during the Alpine cycle of the eastern Iberian basin», *Tectonophysics*, 228, 33-55.

SALVANY, J. (1990), «Las formaciones Falces y Lerin (Oligoceno-Mioceno Continental de Navarra)», in *Formaciones evaporíticas de la Cuenca del Ebro, Cadenas Periféricas y de la zona de Levante*, Orti, F. & Salvany, J. M. (eds.), Enresa-GPPC, Barcelona, 106-115.

SÁNCHEZ-MOYA, Y., SOPEÑA, A, MUÑOZ, A. & RAMOS, A. (1992), «Consideraciones teoricas sobre el análisis de la subsidencia: aplicaciones a un caso real en el borde de la cuenca triásica ibérica», *Rev. Soc. Geol. España*, 5, 21-40.

SCHMOKER, J. W. (1979), «Determination of organic content of Appalachian Devonian shales from formation-density logs», *Amer. Assoc. Petrol. Geol. Bull.*, 63, 1504-1537.

— (1981), «Determination of organic-matter content of Appalachian Devonian shales from gamma-ray logs», *Amer. Assoc. Petrol. Geol. Bull.*, 65, 1285-1298.

SEGURA, M. y WIEDMANN, J. (1982), «La transgresión del Cretácico superior en el Sector de Atienza-Sigüenza (Guadalajara, Cordillera Ibérica) y el significado de la fauna ammonitífera», *Cuad. Geol. Ibérica*, 8, 293-307.

SOPEÑA, A. (1973), *Estratigrafía del borde mesozoico, en el sector de Tamajón-Pinilla de Jadraque,* Tesis de Licenciatura, Universidad Complutense de Madrid (Inédita), 121 pp.

— VIRGILI, C., HERNANDO, S. & RAMOS, A. (1977), «Pérmico continental en España», *Cuad. Geol. Ibérica*, 4, 11-34.

— LÓPEZ, J., ARCHE, A., PÉREZ-ARLUCEA, M., RAMOS, A., VIRGILI, C. & HERNANDO, S. (1988), «Permian and Triassic rift basins of the Iberian Peninsula», *Dev. Geothec.*, 22-B, 757-786.

STECKLER, M. & WATTS, A. (1978), «Subsidence of the Atlantic-type continental margin of New York», *Earth Planet. Sci. Letters*, 41, 1-13.

TISSOT, B. & ESPITALIÉ, J. (1975), «L'evolution thermique de la materie organique des sediments. applications d'une simulation mathématique», *Rev. Inst. Franc. Petrol.*, 30, 743-777.

— PELET, R. & UNGERER, P. (1987), «Thermal history of sedimentary basins, maturation indices, and kinetics of oil and gas generation», *Amer. Assoc. Petrol. Geol. Bull.*, 71, 1445-1466.

— & WELTE, D. (1984), *Petroleum Formation and Occurrence*, Springer-Verlag, New York, 699.

UNGERER, P., BURRUS, J., DOLIGEZ, B., CHÉNET, Y. & BESSIS, F. (1990), «Basin Evaluation by integrated two-dimensional modelling of heat transfer, fluid flow, hydrocarbon generation and migration», *Amer. Assoc. Petrol. Geol. Bull.*, 73, 309-335.

UNGERER, P. & PELET, R. (1987), «Extrapolation of the kinetics of oil and gas formation from laboratory experiments to sedimentary basin», *Nature*, 327, 52-54.

VÁZQUEZ, F. (1981), *El Triásico del anticlinal de Honrubia y su límite con el Jurásico (prov. de Segovia y Burgos),* Tesis de Licenciatura, Universidad Complutense de Madrid (inédita), 135 pp.

WAPLES, D. W., SUIZU, M. y KAMATA, H. (1992 a), «The Art of Maturity Modelling. Part 1. Finding a Satisfactory Geologic Model», *Amer. Assoc. Petrol. Geol. Bull.*, 76, 31-46.

— (1992 b), «The Art of Maturity Modelling. Part 2. Alternative Models and Sensitivity Analysis», *Amer. Assoc. Petrol. Geol. Bull.*, 76, 47-66.

WILDE, S. (1990), «The Bathonian and Callovian of the Northwest-Iberian Range. Stages of facial and paleogeographical differentiation on an epicontinental platform», *Cuad. Geol. Ibérica*, 14, 113-142.

WILLIAMSON, M. A. (1992), «The subsidence, compaction, thermal and maduration history of the Egret Member source rock, Jeanne d'Arc Basin, offshore Newfoundland», *Bull. Can. Petrol. Geol.*, 40, 136-150.

ZIEGLER, P. (1990), *Geological atlas of western and central Europe*, Shell International Petroleum Maatschappij B.V, The Hague, 239 pp.

Manuscrito recibido: 10-5-1996.
Manuscrito aceptado: 26-9-1996.